A&A 570, A74 (2014)
DOI: 10.1051/0004-6361/201424175

Astronomy & Astrophysics

The VMC Survey

XII. Star cluster candidates in the Large Magellanic Cloud⋆

Andrés E. Piatti[1,2], Roald Guandalini[3], Valentin D. Ivanov[4], Stefano Rubele[5], Maria-Rosa L. Cioni[6,7], Richard de Grijs[8,9], Bi-Qing For[10], Gisella Clementini[11], Vincenzo Ripepi[12], Peter Anders[13], and Joana M. Oliveira[14]

[1] Observatorio Astronómico, Universidad Nacional de Córdoba, Laprida 854, 5000 Córdoba, Argentina
e-mail: andres@oac.uncor.edu
[2] Consejo Nacional de Investigaciones Científicas y Técnicas, Av. Rivadavia 1917, C1033AAJ, Buenos Aires, Argentina
[3] Instituut voor Sterrenkunde, Celestijnenlaan 200 D BUS 2401, 3001 Heverlee, Belgium
[4] European Southern Observatory, Av. Alonso de Córdoba 3107, Casilla 19, Santiago, Chile
[5] INAF, Osservatorio Astronomico di Padova, vicolo dell' Osservatorio 5, 35122 Padova, Italy
[6] University of Hertfordshire, Physics Astronomy and Mathematics, College Lane, Hatfeild AL10 9AB, UK
[7] Leibniz-Institut für Astrophysik Potsdam, An der Sternwarte 16, 14482 Potsdam, Germany
[8] Kavli Institute of Astronomy and Astrophysics, Peking University, Yi He Yuan Lu 5, Hai Dian District, Beijing 100871, PR China
[9] Department of Astronomy, Peking University, Yi He Yuan Lu 5, Hai Dian District, 100871 Beijing, PR China
[10] ICRAR, University of Western Australia, 35 Stirling Hwy, Crawley, WA 6009, Australia
[11] INAF, Osservatorio Astronomico di Bologna, via Ranzani 1, 40127 Bologna, Italy
[12] INAF, Osservatorio Astronomico di Capodimonte, via Moiariello 16, 80131 Napoli, Italy
[13] National Astronomical Observatories, Chinese Academy of Sciences, 20A Datun Road, Chaoyang District, 100012 Beijing, PR China
[14] Lennard-Jones Laboratories, School of Physical and Geographical Sciences, Keele University, ST5 5BG, UK

Received 10 May 2014 / Accepted 18 July 2014

ABSTRACT

Context. In this work we analyse colour-magnitude diagrams (CMDs) of catalogued star clusters located in the Large Magellanic Cloud (LMC), from a YJK_s photometric data set obtained by the Visible and Infrared Survey Telescope for Astronomy (VISTA) survey of the Magellanic Clouds system (VMC).
Aims. We studied a total of 98 objects of small angular size, typically ∼11.6 pc in diameter projected towards both uncrowded tile LMC 8_8 and crowded tile LMC 5_5. They populate relatively crowded LMC fields with significant fluctuations in the stellar density, the luminosity function, and the colour distribution as well as uncrowded fields. This cluster sample is aimed at actually probing our performance in reaching the CMD features of clusters with different ages in crowded and uncrowded fields.
Methods. We applied a subtraction procedure to statistically clean the cluster CMDs from field star contamination. We then matched theoretical isochrones to the background-subtracted CMDs to determine the ages and metallicities of the clusters.
Results. We estimated the ages of 65 clusters, which resulted to be in the age range $7.3 < \log(t/\mathrm{yr}) < 9.55$. We also classified as chance grouping of stars 19 previoulsy catalogued clusters, two possible cluster-like asterisms, and one unresolved cluster. For eight other objects, we could not find a clear star concentration in the K_s images either, so we quoted them as cluster-like asterisms. Finally, we found two previously catalogued single star clusters to be unresolved background galaxies (KMHK747, OGLE366), and one to be a triple cluster system (BSDL 2144).

Key words. techniques: photometric – Magellanic Clouds – galaxies: clusters: general

1. Introduction

The Magellanic Clouds are the nearest example of interacting dwarf irregular galaxies. Because of their distance (50−60 kpc) we can resolve individual stars in the field population and in star clusters. Compared to the Milky Way, the Magellanic Clouds have a lower metallicity and host star clusters spanning the entire age range (de Grijs & Anders 2006; de Grijs & Goodwin 2008). The Magellanic Clouds contain a few thousands star clusters (Bica et al. 2008, hereafter B08) and represent an important laboratory for studies of stellar evolution. The sample of star clusters with measurements of size, mass, and other parameters is, however, modest and corresponds to less than half the number of candidate star clusters (e.g. Hill & Zaritsky 2006; Werchan & Zaritsky 2011; Glatt et al. 2010; Baumgardt et al. 2013; Piatti 2014).

Taking advantage of the high sensitivity and spatial resolution of the VISTA near-infrared YJK_s survey of the Magellanic Clouds system (VMC; Cioni et al. 2011) we embarked on a homogeneous determination of star cluster parameters. Compared to the wide-scale Magellanic Clouds Photometric Survey data (Zaritsky et al. 2002, 2004) the VMC survey data corresponds to an improvement of about a factor of two in pixel scale and seeing. In addition, the VMC makes use of the near-infrared filters, YJK_s, covers a wider area around each Cloud, and includes the Magellanic Bridge. The VMC covers ∼170 deg^2 of

⋆ Based on observations made with VISTA at the Paranal Observatory under programme ID 179.B-2003.

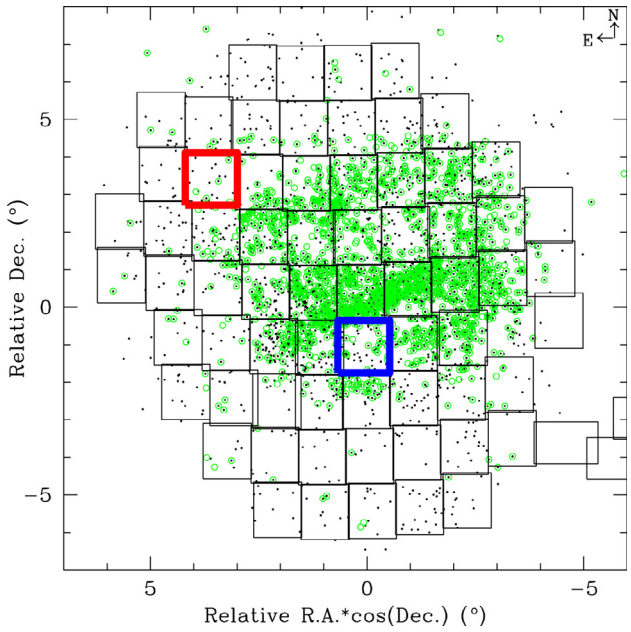

Fig. 1. Sky-projected spatial distribution of the B08 catalogue of star clusters in the LMC centred at RA = 05:23:34, Dec = −69:45:22 (J2000). Black points and green circles represent catalogued star clusters and those with age estimates available, respectively. The objects studied in this work are placed in tiles LMC 5_5 (blue rectangle) and LMC 8_8 (red rectangle).

the entire Magellanic system with 110 individual tiles; each tile covers ∼1.5 deg^2. With a statistical sample of characterised star clusters that is as complete as possible we will be able to answer some important open questions in star cluster studies, such as: Has the field experienced the same star formation history as the cluster stellar population? What is the distribution of star clusters as a function of age and metallicity? What galaxy structure is defined by star clusters with different ages? Is there a relation between the age and size of star clusters?

This is the first VMC paper that provides information on the star clusters of the Magellanic system. Some preliminary results from the analysis of star clusters in a tile covering the south ecliptic pole (SEP) region are published in Cioni et al. (2011). The complete study of star clusters in the SEP tile (tile LMC 8_8) is presented here along with analysis of clusters in tile LMC 5_5 covering the LMC bar. Study of star clusters in other tiles will follow. We plan to study known star clusters identified in previous studies, and included in the B08 catalogue, and to search for new star clusters based on the stellar surface density method (Ivanov et al. 2002; Borissova et al. 2003). Figure 1 depicts the spatial distribution of the B08 catalogue of star clusters, where black points and green circles represent the B08 catalogued star clusters and those with age estimates available. The VMC tile distribution is superimposed.

This paper is organised as follows. The VMC observations and data reduction are presented in Sect. 2. The star cluster sample is described in Sect. 3, while the cleaning of the colour-magnitude diagrams (CMDs) and the derivation of the cluster parameters (size, age, metallicity) are presented in Sects. 4 and 5, respectively. Finally, we discuss the results in Sect. 6 and draw our main conclusions of this analysis in Sect. 7.

2. Data collection and reduction

The VMC survey strategy involves repeated observations of tiles across the Magellanic system, where one tile covers uniformly an area of ∼1.5 deg^2, as a result of the mosaic of six paw-print images, in a given waveband with 3 epochs at Y and J, and 12 epochs at K_s. Individual epochs have exposure times of 800 s (Y and J) and 750 s (K_s). The average quality of the VMC data analysed here corresponds to 0.34″ pixel size, 0.90″ FWHM, and 0.06 ellipticity.

To date eleven tiles in the LMC have been completely observed; three of them are located in the innermost region of the LMC, nominally the tiles LMC 6_6, 6_4, and 5_5. The tile LMC 6_6 (30 Doradus) is a high rate star formation region affected by large differential extinction (see e.g. Rubele et al. 2012; Tatton et al. 2013); the tile LMC 6_4 is located in the centre of the LMC Bar with high levels of crowding that could affect the capability of our tools to detect stars in clusters and decontaminate them by the LMC background stars. Star clusters in these central tiles will be analysed separately.

Tile LMC 5_5 is located towards the LMC outer Bar/Bar region (centred at RA = 05:24:30, Dec = −70:48:34 (J2000)) and contains 77 catalogued clusters with a noticeable field star crowding level and moderate extinction. It was completed early in the course of the survey, and we obtained point-spread function (PSF) photometry of the clusters in this tile. Consequently, we can probe our performance in reaching the main sequence turnoffs (MSTOs) of intermediate-age and relatively old clusters in crowded fields. Our previous experience (Cioni et al. 2011; Rubele et al. 2012) shows that the widest colour range of the $Y - K_s$ colour is best for cluster studies because it makes it easier to distinguish different cluster main sequences (MSs), particularly their turnoff regime, and the red giant phases, as well as having a higher sensitivity to reddening and metallicity than the $Y - J$, and $J - K_s$ colours. Therefore, the present analysis mainly relies on the K_s versus $Y - K_s$ CMDs; the J versus $Y - J$ and K_s versus $J - K_s$ CMDs are useful in order to confirm our results.

Tile LMC 8_8 was one of the first two fully completed VMC survey tiles, and it overlaps with the SEP field. The tile is centred at RA = 05:59:23, Dec = −66:20:28 (J2000) and includes 23 catalogued clusters, of which two are binary clusters (KMHK 1552 + BSDL 3190, and KMHK 1519 + BSDL 3174; Dieball et al. 2002). The clusters catalogued by B08 located within the limits of tiles LMC 5_5 and 8_8 are listed in Table 1 (see also Fig. 1).

The tile LMC 5_5 and 8_8 data refers to observations acquired from November 2009 to December 2012 under homogeneous sky conditions since it was obtained in service mode when the sky quality met the requested VMC criteria (see Cioni et al. 2011). The data were reduced with the VISTA Data Flow System pipeline, version 1.1 (VDFS; Irwin et al. 2004), and calibrated into the VISTA photometric system, which is close to the Vegamag system; we extracted it from the VISTA Science Archive (VSA; Cross et al. 2012).

For this work we perform our PSF photometry on a homogenised VMC deep tile image, that was created starting from the paw-print VMC images. The PSF homogenised methodology consists in a convolution with a kernel of the original paw-print images to turn different PSF shapes into a more constant and uniform PSF model on the paw-print images. The purpose of degrading the PSF on paw-print images, to a unique PSF model, is to produce deep tile images with a uniform and homogeneous PSF. Actually the paw-print images are stacked single exposures reaching a continuous observation time of a hundred seconds, therefore variations of the seeing occurring over these timescales could affect the PSF shape on the final deep tile as a function of the position.

Table 1. Fundamental parameters of the studied LMC cluster candidates.

ID	RA (°)	Dec (°)	r (′)	$E(B-V)$ (mag)	log(t/yr)	[Fe/H] (dex)	Notes
				LMC 5_5			
BSDL 1504	80.775	–71.422	0.4	0.065	9.55	–0.7	
BSDL 1355	80.342	–70.900	0.4	0.064	9.50	–0.7	
BSDL 1341	80.249	–70.318	0.5	0.085	9.45	–0.7	
SL 435	80.875	–71.428	0.4	0.065	9.40	–0.7	8.70 ± 0.20, –0.4 (1)
KMHK 897	81.492	–70.459	0.7	0.085	9.40	–0.7	
KMHK 835	80.533	–71.175	0.5	0.064	9.40	–0.7	
HS 329	82.442	–71.001	0.4	0.070	9.30	–0.7	9.25 ± 0.04 (4)
KMHK 750	79.577	–70.721	0.4	0.086	9.30	–0.4	
SL 472	81.562	–70.380	0.4	0.085	9.20	–0.7	
BSDL 1672	81.375	–71.087	0.25	0.070	9.20	–0.4	
HS 323	82.215	–70.207	0.6	0.071	9.20	–0.4	
HS 264	80.805	–70.778	0.4	0.082	9.10	–0.4	9.20 ± 0.04 (4)
KMHK 997	82.576	–70.420	0.5	0.076	9.10	–0.4	
NGC 1987	81.821	–70.738	0.8	0.080	9.00	–0.4	9.05 ± 0.05, 0.010 (3)
SL 389	79.905	–71.211	0.7	0.064	8.90	–0.4	
HS 214	79.460	–70.801	0.3	0.086	8.90	–0.4	8.15 ± 0.04, –0.4 (1)
KMHK 907	81.553	–70.981	0.3	0.070	8.80	–0.4	
HS 238	80.033	–70.156	0.3	0.100	8.80	–0.4	
SL 441	80.925	–71.037	0.5	0.064	8.80	0.0	
BSDL 2123	82.775	–70.168	0.5	0.071	8.80	–0.4	
SL 399	80.087	–70.768	0.5	0.064	8.50	–0.4	8.30 ± 0.05, –0.4 (1)
KMK 88_55	80.923	–70.096	0.3	0.084	8.50	–0.4	
HS 304	81.814	–71.172	0.4	0.074	8.50	–0.4	
SL 406	80.258	–70.873	0.3	0.064	8.45	–0.4	8.50 ± 0.05, –0.4 (1)
SL 395	79.996	–70.665	0.3	0.083	8.40	–0.4	8.30 ± 0.20, –0.4 (1)
HS 324	82.229	–71.120	0.3	0.070	8.40	–0.4	
SL 364	79.423	–71.066	0.3	0.094	8.30	–0.4	8.00 ± 0.20, –0.4 (1)
NGC 1943	80.623	–70.155	0.5	0.085	8.30	–0.4	8.35 ± 0.05, –0.4 (1)
SL 487e	81.788	–71.023	0.4	0.070	8.30	–0.4	
KMHK 764	79.720	–70.602	0.4	0.091	8.30	–0.4	
SL 431	80.800	–70.2805	0.4	0.050	8.30	–0.4	
NGC 2010	82.641	–70.819	0.5	0.078	8.20	–0.4	8.20 ± 0.05, –0.4 (2)
SL 510	82.340	–70.579	0.5	0.076	8.10	–0.4	8.10 ± 0.10, –0.4 (5)
KMHK 999	82.553	–71.557	0.3	0.076	8.00	–0.4	
BSDL 1949	82.345	–70.237	0.4	0.071	7.70	–0.4	
BSDL 1876	81.977	–71.522	0.2	0.076	7.50	–0.4	8.20 ± 0.40, –0.4 (1)
BSDL 2008	82.460	–71.068	0.3	0.070	7.50	–0.4	
SL 539	82.733	–70.695	0.4	0.078	7.50	–0.4	7.40 ± 0.20, –0.4 (1)
BSDL 2199	82.942	–70.253	0.4	0.071	7.50	–0.4	
KMHK 979	82.412	–70.986	0.4	0.070	7.30	–0.4	7.30 ± 0.40, –0.4 (1)
BSDL 1955	82.332	–71.031	0.3	0.070	7.30	–0.4	7.30 ± 0.40, –0.4 (1)
BSDL 1980	82.387	–70.994	0.5	0.070	7.30	–0.4	7.30 ± 0.40, –0.4 (1)
BSDL 1830	81.892	–70.614	0.2	0.076	7.30	–0.4	7.50 ± 0.60, –0.4 (1)
BSDL 1875	81.976	–71.547	0.3	0.076	7.30	–0.4	8.60 ± 0.60, –0.4 (1)
SL 528	82.670	–70.223	0.2	0.071	>9.00	...	cluster-like asterism?
OGLE 545	82.663	–70.217	0.2	0.071	>9.00	...	cluster-like asterism?
BSDL 1182	79.568	–71.435	0.15	0.065	...	...	unresolved cluster?
HS 232	80.155	–70.964	0.2	0.064	...	...	possible non-cluster; 9.20 ± 0.10, –0.4 (1)
HS 265	80.817	–70.234	0.25	0.085	...	...	possible non-cluster
BSDL 1790	81.720	–70.211	0.4	0.085	...	...	possible non-cluster
OGLE 534	82.515	–70.126	0.2	0.063	...	...	possible non-cluster
OGLE 536	82.517	–70.205	0.2	0.071	...	...	possible non-cluster
KMHK 801	80.114	–70.450	0.3	0.085	...	...	possible non-cluster
HS 295	81.524	–70.092	0.3	0.085	...	...	possible non-cluster
HS 282	81.318	–70.099	0.3	0.085	...	...	possible non-cluster
BSDL 2196	82.932	–70.201	0.2	0.071	...	...	possible non-cluster
BSDL 2063	82.618	–70.560	0.5	0.076	...	...	possible non-cluster
OGLE 471	81.573	–70.222	0.3	0.085	...	...	possible non-cluster
HS 345	82.956	–70.287	0.25	0.071	...	...	possible non-cluster
KMHK 819	80.333	–71.407	0.3	0.065	...	...	possible non-cluster
HS 342	82.940	–70.308	0.3	0.071	...	...	possible non-cluster
SL 542	82.825	–70.216	0.4	0.071	...	...	possible non-cluster

References. (1) Glatt et al. (2010); (2) Gouliermis et al. (2010); (3) Milone et al. (2009); (4) Piatti (2011); (5) Piatti (2012).

Table 1. continued.

ID	RA (°)	Dec (°)	r (′)	$E(B-V)$ (mag)	log(t/yr)	[Fe/H] (dex)	Notes
BSDL 1645	81.336	–71.196	0.4	0.074	...	...	possible non-cluster
GKK O102	82.871	–70.757	0.3	0.078	...	...	possible non-cluster
SL 439	81.010	–70.174	0.3	0.084	...	...	possible non-cluster
BSDL 2202	82.897	–70.735	0.5	0.078	...	...	cluster-like asterism
GKK O15	80.550	–71.319	0.5	0.065	...	...	cluster-like asterism
KMHK 740	79.449	–71.157	0.4	0.064	...	...	cluster-like asterism
OGLE 542	82.642	–70.197	0.4	0.071	...	...	cluster-like asterism
HS 286	81.408	–70.262	0.2	0.085	...	...	cluster-like asterism
GKK O119	80.627	–70.360	0.4	0.085	...	...	cluster-like asterism
GKK O100	82.753	–70.920	0.5	0.078	...	...	cluster-like asterism
BSDL 2144	82.785	–71.131	...	0.070	...	...	possible triple system
KMHK 747	79.519	–71.269	...	0.065	...	...	possible galaxy
OGLE 366	80.033	–70.144	...	0.100	...	...	possible galaxy
				LMC 8_8			
KMHK 1592	90.375	–66.987	0.8	0.042	9.8	–0.7	
KMHK 1521	88.742	–67.114	0.5	0.050	9.5	–0.4	
KMHK 1585	90.212	–66.913	0.5	0.042	9.3	–0.7	
KMHK 1578	89.991	–66.443	0.4	0.035	9.25	–0.7	
KMHK 1552	89.468	–65.950	0.2	0.034	9.2	–0.7	
KMHK 1609	90.795	–65.675	0.4	0.037	9.2	–0.4	
KMHK 1577	89.952	–66.770	0.5	0.042	9.2	–0.4	
KMHK 1623	91.140	–66.442	0.5	0.040	9.2	–0.4	
KMHK 1567	89.703	–66.059	0.5	0.034	9.1	–0.4	
KMHK 1555	89.466	–66.401	0.5	0.035	9.1	–0.4	
KMHK 1597	90.541	–65.776	0.4	0.034	9.1	–0.4	
KMHK 1600	90.619	–66.920	0.4	0.037	9.1	–0.4	
KMHK 1611	90.835	–66.126	0.3	0.037	9.1	–0.4	
BSDL 3174	88.685	–66.715	0.3	0.043	9.1	–0.4	
KMHK 1568	89.695	–66.844	0.3	0.042	9.0	–0.4	
KMHK 1510	88.642	–65.740	0.5	0.035	9.0	–0.4	
LW 334	89.001	–66.288	0.4	0.040	8.9	–0.4	
BSDL 3188	89.325	–66.273	0.5	0.035	8.9	–0.4	
KMHK 1519	88.729	–66.714	0.5	0.043	8.9	–0.4	
KMHK 1516	88.709	–65.838	0.4	0.035	8.8	–0.4	
KMHK 1589	90.329	–66.854	0.6	0.042	8.7	–0.4	
BSDL 3190	89.472	–65.945	0.15	0.034	...	...	asterism
KMHK 1607	90.714	–66.660	0.3	0.039	...	...	possible non-cluster

We performed PSF photometry on the homogenised deep tile image, created as described in Rubele et al. (2012), of VMC tiles LMC 5_5 and 8_8, using the IRAF DAOPHOT packages (Stetson 1987). The PSF model was created using ~2500 stars uniformly distributed and with magnitudes close to the saturation limit + 1.5 mag (for the VMC survey the single paw-print saturation limits are 12.9 mag, 12.7 mag, and 11.4 mag in Y, J, and K_s, respectively). Subsequently, we used the ALLSTAR routine to perform the final PSF photometry on all three filter images, and correlated the resulting catalogues using a one arcsec radius. We checked and corrected our PSF photometry to the aperture effect using catalogs retrieved from the VSA (Lewis et al. 2010; Cross et al. 2012)[1], for the bulk of the observed stars. We ran a large number of artificial star tests (ASTs) to estimate the incompleteness and error distribution of our data for each tile and throughout the CMD. For each region we ran $\sim 20 \times 10^6$ ASTs as described in Rubele et al. (2012), using a spatial grid with 25 pixels in width and with a magnitude distribution proportional to the square of the magnitude. This choice for the magnitude distribution allows us to better map completeness and errors in the less complete regions of the CMD. Figure 2 depicts CMDs for both tiles with error bars coloured according to the colour scale of the completeness level. Photometric errors of 0.10 mag were derived for stars with $Y = 19.95$ mag, $J = 19.78$ mag, and $K_s = 19.27$ mag in the tile LMC 5_5, and $Y = 21.52$ mag, $J = 21.23$ mag, and $K_s = 20.43$ mag in the tile LMC 8_8. As for the photometry completeness we found that our data set is 50% complete at $Y = 20.6$ mag, $J = 20.3$ mag, and $K_s = 19.9$ mag in the tile LMC 5_5, and at $Y = 22.1$ mag, $J = 21.7$ mag, and $K_s = 20.6$ mag in the tile LMC 8_8.

3. The cluster sample

We analysed a total of 98 (75 in LMC 5_5 and 23 in LMC 8_8) candidate clusters spread over the area covered by the tiles considered. They are all the objects catalogued by B08 which overlap the tile areas, in addition to BSDL 2147 and BSDL 2221 in LMC 5_5, which we discarded because they fall in a small tile region affected by dead pixels and on the edge of the tile, respectively. The studied objects range from intermediate-age cluster candidates (age $\leq$ 6 Gyr) to very young clusters (age ~20 Myr). We also confirmed that some of the previously catalogued clusters are not actually real stellar aggregates, but are possible cluster-like asterisms (see Sect. 6). Furthermore, the angular resolution of VMC made it apparent that two catalogued clusters (KMHK747 and OGLE366 in LMC 5_5) are most likely

[1] http://horus.roe.ac.uk/vsa/

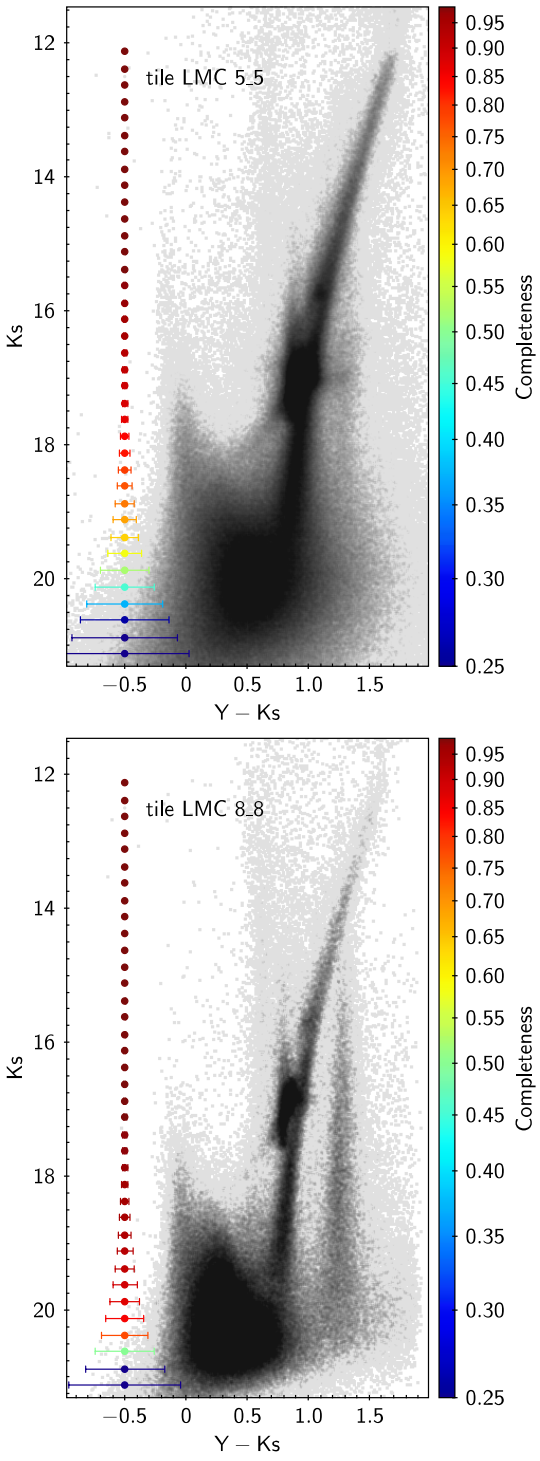

Fig. 2. CMDs for stars in tiles LMC 5_5 and 8_8 with error bars coloured according to the colour scale of the completeness level.

compact galaxies. Consequently, the analysis of the candidate clusters allowed us to attain a more robust cluster sample with genuine physical systems in this particular field. We also refer the reader to the work by Piatti (2014) for a discussion on the completeness of the presently known star cluster population.

The confirmed clusters with ages larger than 1 Gyr will allow us to explore overall features related to the star formation and chemical evolution history of the LMC. For instance, an important burst of cluster formation took place ∼2 Gyr ago after a cluster age gap (Piatti 2011; Piatti et al. 2002). On the other hand, younger clusters have been studied in the context of a variety of different astrophysical issues, like the initial mass function, the recent star formation rate, the early star cluster disruption (Da Rio et al. 2009; Indu & Subramaniam 2011; de Grijs et al. 2013), among others. The accuracy of the astropysical properties derived of clusters covering a wide age range allows us to assess the ability of the VMC survey in dealing with such a variety of objects, particularly those of relatively small angular size and projected towards crowded regions such as in the LMC outer Bar.

In order to avoid mismatching between the observed objects and the actual list of catalogued clusters, we first overplotted the positions of catalogued clusters (B08) to the deepest K_s image. Thus, by using the names and the coordinates provided by B08, we recognised the observed clusters one by one in the K_s image. Then, we searched for such clusters in the Digitized Sky Survey (DSS)[2] because they were originally identified from optical data – and downloaded $15' \times 15'$ B images centred on the coordinates matched by the DSS. We also used the SIMBAD Astronomical Database as an additional source for checking cluster coordinates. Finally, we compared the DSS extracted regions with the respective ones in the K_s VMC survey. We are confident of the matching procedure, particularly when dealing with multiple cluster systems. We note that most of the observed objects are of small angular size, typically ∼0.8′ in diameter (∼11.6 pc), and are projected towards relatively crowded fields with significant stellar density fluctuations. Such adverse physical conditions made it harder not only to distinguish a star cluster from a chance grouping of stars, but also to realiably determine the cluster centres.

4. Cleaning the cluster colour–magnitude diagrams

The catalogued cluster candidates appear in the sky as small concentrations of stars that do not necessarily lead to the conclusion that such concentrations constitute real physical systems. They may imply that we are dealing with the presence of a genuine star cluster, a chance grouping of stars along the line of sight or a non-uniform distribution of interstellar material in that surveyed region. The CMDs of the stars located within a region around the catalogued cluster centres are a helpful tool in order to assess the real entity of the objects. Nevertheless, given the significant fluctuations seen in the stellar density in that part of the LMC as well as in the luminosity function and in the colour distribution, the CMDs alone might lead to incorrect interpretations (Nikolaev & Weinberg 2000; van der Marel 2001). In general, the extracted CMDs are the result of the composite stellar population distributed along the line of sight.

For this reason, we employed a cleaning procedure that compares the extracted CMD centred on the cluster coordinates to four distinct CMDs built from field stars located reasonably far beyond the object, but not so far as to lose the local star field signature in terms of stellar density, luminosity function and colour distribution. As a rule, the cluster region encompassed a circular area with a radius 3 times that of the cluster; the cluster's radius was taken either from a visual inspection of the deepest K_s image (where the profile disappears into the background noise) or from B08 or from both sources combined. The four field regions were designed to have an equal cluster area, and were placed to

[2] The Digitized Sky Surveys were produced at the Space Telescope Science Institute under US Government grant NAG W-2166. The images of these surveys are based on photographic data obtained using the Oschin Schmidt Telescope on Palomar Mountain and the UK Schmidt Telescope. The plates were processed into the present compressed digital form with the permission of these institutions.

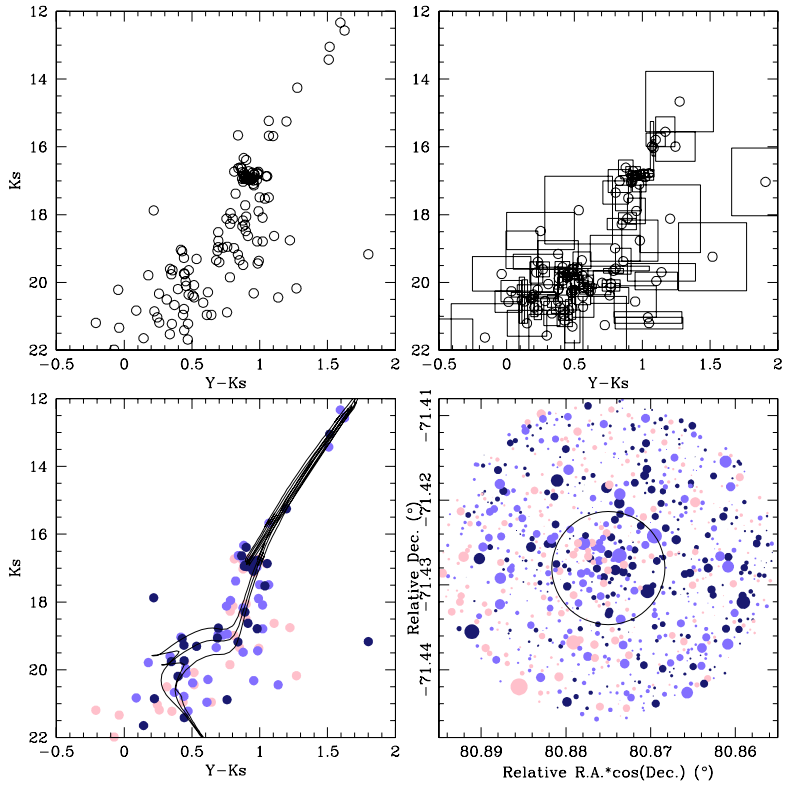

Fig. 3. CMDs for stars in the field SL 435 (LMC 5_5): the observed CMD for the stars distributed within the cluster radius (*top left panel*); a field CMD for an annulus centred on the cluster, with an internal radius 3 times the cluster radius and an area equal to that of the cluster area (*top right panel*); the cleaned cluster CMD (*bottom left*). We overplotted box-shaped cells for each star in the field CMD to be used in the cluster CMD field decontamination (see section 4 for details). Colour-scaled symbols represent stars that statistically belong to the field ($P \leq 25\%$, pink), stars that might belong either to the field or to the cluster ($P = 50\%$, light blue), and stars that predominantly populate the cluster region ($P \geq 75\%$, dark blue). Three isochrones from Marigo et al. (2008) for log (t/yr), log (t/yr) ± 0.1, and metallicity values listed in Table 1 are also superimposed. The schematic chart centred on the cluster for a circle of radius 3 times the cluster radius is shown in the *bottom right panel*. The black circle represents the adopted cluster radius. Symbols are as in the bottom left panel and with a size proportional to the brightness of the star. North is upwards, and east is to the left.

the north, to the east, to the south, and to the west next to the cluster area. We statistically reproduced the four field CMDs by means of box-shaped cells of different dimensions, whose positions and sizes were defined from the field CMDs, and then used them to clean the cluster CMD by subtracting one star per box-shaped cell; the chosen star was located within the cell and closest to its centre. We refer the reader to Piatti & Bica (2012, see their Fig. 12 which illustrates the cell definition) for a detailed description of the field star cleaning procedure.

The method relies on the fact that some parts of the field CMD are more populated than others, so that counting the number of stars within boxes of a fixed size becomes a less effective task. In general, bigger boxes are required to satisfactorily reproduce CMD regions with a small number of field stars, while smaller boxes are necessary in populous CMD regions. For instance, relatively bright field red giants with small photometric errors can be subtracted only if large enough boxes are used, so that a cluster CMD without such feature a spurious red giant can be built.

The method assumes that the cells defined on the field CMDs vary in magnitude and colour separately. This is done by starting with a reasonably big box $((\Delta K_s, \Delta(Y - K_s)) = (1.00, 0.25)$ mag) centred on each field star and then by reducing its size until it reaches the star closest in magnitude and that closest in colour, respectively, so that it is bigger in CMD regions with a small number of stars, and vice versa (see Fig. 3, top right panel). Then, all of the designed cells are plotted over the cluster CMD and the closest stars to each cell centre in the cluster CMD is eliminated independently of possible overlapping cells.

We performed the background subtraction four times per cluster, once for each field region. When comparing the four resulting decontaminated cluster CMDs, we find stars that have been kept unsubtracted different times. The different number of times that a star keeps unsubtracted can then be converted in a measure of the probability of being a fiducial feature of the cleaned region. Thus, we are able to distinguish field populations projected on the cluster area, i.e. those with a probability of being a fiducial feature $P \leq 25\%$; stars that could indistinguishably belong to the field or to the studied object ($P = 50\%$); and stars that are predominatly found in the cleaned area ($P \geq 75\%$) rather than in the star field population.

To illustrate the performance of the cleaning procedure, we show in Fig. 3 a schematic chart for the SL 435 field (bottom right); the extracted cluster CMD for the stars distributed within the circle drawn in the schematic chart (top left panel); a single field CMD for an annulus centred on the cluster, with an internal radius 3 times that of the circle drawn in the schematic chart and an area equal to that used to build the cluster CMD (top right); and the cleaned cluster CMD (bottom left). We overplotted on the field CMD the cells designed for each star, which are thought to be superimposed on the cluster CMD in order to eliminate from it one star per cell, specifically those closest to their respective cells' centres. The colour scale used for the symbols in the bottom panels represents stars that statistically belong to the field ($P \leq 25\%$, pink), stars that might belong either to the field or to the cluster ($P = 50\%$, light blue), and stars that predominantly populate the cluster region ($P \geq 75\%$, dark blue). We note that the cluster region has more red clump, lower and upper red giant branch stars, as well as a less populated MS than the field. A full sample of figures for the remaining studied objects is provided with the on-line version of the Journal.

It is apparent from some CMDs that the stars with the highest cluster membership probability (dark blue filled circles) do not define traceable cluster sequences in the CMD and/or are not concentrated within the circular cluster areas. Particularly, residuals at the red clump (RC), subgiant branch, and the lower MS are visible. For this reason, when sizing up whether the clusters are real and estimating their fundamental parameters, we used at the same time the information coming from the CMD and from the spatial distribution, i.e. we tried to make compatible the conclusions drawn separately from the analysis of both bottom panels in the produced figures. We also examined the cluster nature

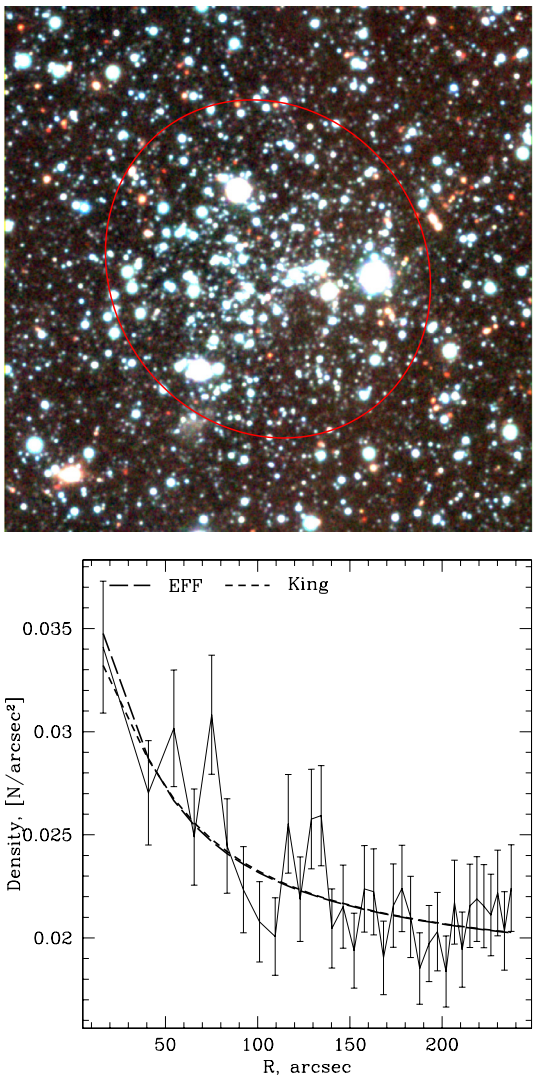

Fig. 4. *Top*: three-colour composite 3 × 3 arcmin image of KMHK 1592 (LMC 8_8) (Y – blue, J – green, K_s – red; north is up and east is to the left.). *Bottom*: profiles of KMHK 1592 obtained from the King and EFF models compared with the data.

of the catalogued objects and their dimensions on the K_s and DSS images. We usually marked on them the stars with different probabilities P(%), recognised unresolved objects, and estimated the reachable limiting magnitude.

Measuring the cluster sizes proved particularly challenging. We could not estimate them by fitting the radial profile with King's or other profiles because most of the clusters are remarkably small and/or have very few possible members which makes it difficult to build stellar radial profiles (see next section). Instead, we adopted radii that are a compromise between maximising the number of stars with $P > 75\%$ and minimising those with $P \leq 50\%$ in the CMD and in the sky, simultaneously. The reached limiting magnitude to resolve stars also played an important role. Fortunately, there are some clusters in our sample with available CMDs in the literature which we used for comparison purposes (HS 329, HS 264, NGC 1987, SL 510). The central coordinates and radii of all the cluster candidates are listed in Table 1.

4.1. Stellar profile fitting

Our first step to determine the structural parameters of the clusters was to build their stellar density profiles after the field decontamination, since the background is not uniform at the spatial scale of the cluster, and therefore it does not add a constant to the surface density profile.

First, we re-determined the centre of each cluster by averaging the coordinates of all the VMC survey stars within the ellipse given by B08. Once the tidal radius was calculated (see below), the centre was re-determined. The procedure was repeated a few times, until the position was stable to within 1/1000 deg. Our final coordinates agree well with the B08 values to within (5 ± 3) arcsec.

Next, we fitted the classical King (1962) and EFF (Elson et al. 1987) profiles, given by:

$$n(r) = k \times \left\{1/\left[1 + (r/r_0)^2)\right]^{1/2} - (1/\left[1 + (r_t/r_0)^2\right]^{1/2}\right\}^2 + \phi_K \quad (1)$$

and

$$n(r) = n_0 \times \left\{1 + (r/a)^2\right\}^{-\gamma/2} + \phi_E, \quad (2)$$

respectively. Here, $n(r)$ is the number of stars per unit area as a function of the radius r; k and n_0 are central projected stellar number densities; r_0 is the King's radius; a is a core parameter, related to the core radius r_c,

$$r_c = a \times (2^{2/\gamma} - 1)^{1/2}; \quad (3)$$

r_t is the tidal radius; and ϕ_K and ϕ_E are background stellar number densities. We also calculated the concentration parameter c:

$$c = \log(r_t/r_0). \quad (4)$$

Table 2 presents the results from these fits for 30 clusters for which the fitting method converged, while Fig. 4 shows an example of radial and fitted profiles. Most of the clusters in the tile LMC 5_5 are of small angular size, contain a few stars, and are projected towards relatively crowded star fields as well, which mainly prevented the fitting procedure from converging. For comparison, we list the cluster sizes from Bica et al. (2008) and Kontizas et al. (1990), converted into arcsec. Finally, we explored the ellipticity of the clusters, fitting ellipses to the radial profile, but the typical deviation from a circular shape was ≤10%, comparable to the uncertainty in the cluster sizes, so we refrained from further investigation of the two-dimensional cluster shapes.

Unfortunately, for many clusters (and particularly for the smaller ones) we obtain values of the tidal radius r_t that are unreliable and so large (≥100 arcsec) that it become meaningless to exploit for the isochrone fitting; possibly because many clusters in the sample are small and do not have enough stars to build reliable stellar radial profiles.

5. Fundamental parameters of the clusters

In order to estimate ages for the catalogued cluster sample, we first adopted appropriate reddening from the available reddening maps, and a distance modulus equal to that of the LMC, and then fitted theoretical isochrones covering a wide range in age and metallicity to the probable ($P \geq 75\%$) cluster members on the K_s versus $Y-K_s$ CMDs. The colour excesses and the distance modulus played a double role. On the one hand, they made the number of variables to be considered in the theoretical isochrone fits smaller. Instead of simultaneously varying four parameters, we only looked for the age and the metallicity of the isochrone which best matched the cluster features. On the other hand, they served as an external control of the zero point of our photometry. Fortunately, in all the analysed CMDs, the zero age main

Table 2. Elson-Fall-Freeman and King's profile fitting results.

Cluster ID	Elson-Fall-Freeman profile			King profile			Bica		Kontizas
	γ	a	r_c	r_0	r_t	c	Maj	Min	
		arcsec	arcsec	arcsec	arcsec		arcsec		
LMC 5_5									
BSDL 1341	...	...	...	...	...	...	33	30	...
BSDL 1355	...	...	...	...	...	...	36	33	...
BSDL 1504	...	...	...	...	...	...	30	24	...
BSDL 1672	...	...	...	...	...	...	36	33	...
BSDL 2123	...	...	...	...	...	...	66	51	...
HS 214	0.4 ± 0.1	0.6 ± 0.2	2.6 ± 1.8	...	...	...	27	21	20.1
HS 238	...	...	...	...	...	...	48	39	...
HS 304	...	...	...	...	...	...	60	60	60.3
HS 323	...	...	...	...	...	...	39	30	...
HS 324	...	...	...	...	...	...	48	39	40.2
HS 329	0.3 ± 0.1	1.8 ± 0.8	17.0 ± 23.2	1.4 ± 0.1	6.7 ± 0.1	0.7 ± 0.1	45	39	46.8
KMHK 750	0.4 ± 0.1	0.9 ± 0.3	5.6 ± 3.0	2.8 ± 0.1	13.0 ± 0.1	0.7 ± 0.1	48	36	33.6
KMHK 835	0.3 ± 0.1	2.1 ± 0.6	17.2 ± 9.9	4.0 ± 0.9	105.1 ± 18.0	1.4 ± 0.2	54	48	40.2
KMHK 897	...	...	...	...	...		36	30	26.7
KMHK 907	0.8 ± 0.1	1.0 ± 0.3	2.2 ± 0.7	0.8 ± 0.1	13.0 ± 1.7	1.2 ± 0.1	33	30	40.2
KMHK 997	...	...	...	...	...	...	54	39	40.2
KMK 88_55	...	...	...	...	...	...	36	30	...
NGC 1987	0.3 ± 0.1	3.7 ± 1.0	32.5 ± 19.0	2.6 ± 0.1	17.5 ± 0.3	0.8 ± 0.1	102	102	98.4
SL 389	0.8 ± 0.1	6.8 ± 1.4	13.4 ± 4.6	3.3 ± 0.1	23.8 ± 0.6	0.9 ± 0.1	96	78	100.5
SL 399	0.6 ± 0.1	1.2 ± 0.2	3.5 ± 0.9	2.1 ± 0.1	16.0 ± 0.3	0.9 ± 0.1	66	60	46.8
SL 435	0.6 ± 0.1	9.0 ± 2.8	22.6 ± 13.9	3.3 ± 0.1	23.6 ± 0.6	0.9 ± 0.1	57	54	73.4
SL 441	...	...	...	...	...	...	54	54	46.8
SL 472	...	...	...	...	...	...	60	51	100.5
LMC 8_8									
KMHK 1510	0.7 ± 0.2	2.1 ± 1.5	4.2 ± 5.7	20.0 ± 0.9	227.1 ± 9.1	1.1 ± 0.1	27	24	26.7
BSDL 3174	3.2 ± 1.0	23.1 ± 5.7	13.8 ± 7.3	3.5 ± 0.1	38.0 ± 1.0	1.0 ± 0.1	39	33	...
KMHK 1516	4.6 ± 1.5	34.6 ± 7.6	16.7 ± 8.0	5.5 ± 0.3	84.0 ± 4.2	1.2 ± 0.1	72	72	60.3
KMHK 1519	1.0 ± 0.1	9.1 ± 2.5	13.9 ± 6.2	18.0 ± 0.4	181.0 ± 4.0	1.0 ± 0.1	39	39	46.7
KMHK 1521	2.1 ± 0.2	43.1 ± 5.2	38.4 ± 8.2	19.0 ± 0.3	200.1 ± 2.9	1.0 ± 0.1	72	66	53.3
LW 334	1.9 ± 0.4	7.5 ± 2.1	6.5 ± 3.3	4.0 ± 0.4	73.5 ± 5.7	1.3 ± 0.1	36	33	...
BSDL 3188	1.2 ± 0.4	8.0 ± 3.8	9.1 ± 8.2	19.0 ± 0.6	212.2 ± 6.6	1.1 ± 0.1	51	42	...
KMHK 1555	1.5 ± 0.1	25.0 ± 3.2	28.9 ± 6.0	12.5 ± 0.9	209.0 ± 10.2	1.2 ± 0.1	90	90	80.4
KMHK 1552	7.3 ± 3.7	43.0 ± 11.9	14.7 ± 10.0	3.0 ± 0.1	30.0 ± 0.7	1.0 ± 0.1	60	51	60.3
KMHK 1568	...	...	...	...	...	...	30	27	33.6
KMHK 1567	1.3 ± 0.2	14.0 ± 3	16.5 ± 7.5	11.0 ± 0.8	177.0 ± 10.3	1.2 ± 0.1	57	48	40.2
KMHK 1577	1.8 ± 0.5	13.5 ± 4.3	11.5 ± 7.3	6.0 ± 0.5	107.3 ± 7.9	1.3 ± 0.1	45	42	60.3
KMHK 1578	...	...	...	...	...	...	54	45	40.2
KMHK 1585	1.1 ± 1.2	2.0 ± 1.9	1.5 ± 3.7	9.0 ± 1.1	182.4 ± 21.3	1.3 ± 0.2	39	36	40.2
KMHK 1589	4.9 ± 1.4	37.5 ± 7.3	18.1 ± 7.5	4.5 ± 0.2	65.0 ± 2.1	1.2 ± 0.1	66	60	80.4
KMHK 1592	0.9 ± 0.1	23.5 ± 2.6	43.8 ± 8.0	33.0 ± 0.4	247.0 ± 3.0	0.9 ± 0.1	132	114	100.5
KMHK 1597	5.0 ± 1.4	22.0 ± 3.9	10.4 ± 3.9	2.5 ± 0.1	35.0 ± 1.4	1.2 ± 0.1	60	54	46.7
KMHK 1600	...	...	...	...	...	...	66	66	46.7
KMHK 1607	8.0 ± 3.7	20.0 ± 5.0	6.7 ± 4.1	0.9 ± 0.1	14.0 ± 1.0	1.2 ± 0.2	48	39	53.3
KMHK 1609	1.4 ± 0.2	20.7 ± 3.8	24.6 ± 7.4	16.0 ± 0.4	193.2 ± 4.2	1.1 ± 0.1	90	84	93.5
KMHK 1611	1.0 ± 0.1	5.0 ± 1.5	7.3 ± 3.4	10.5 ± 0.9	202.2 ± 14.4	1.3 ± 0.2	39	33	40.2
KMHK 1623	2.6 ± 0.5	15.5 ± 2.7	11.4 ± 3.8	3.5 ± 0.3	63.5 ± 3.7	1.3 ± 0.1	72	72	53.3

Notes. The 1σ errors are listed. For comparison we list the cluster sizes from Bica et al. (2008) and Kontizas et al. (1990) in arcsec. The sizes of Kontizas et al. (1990) were converted from pc to arcsec units using a LMC distance modulus of $\mu = 18.49$ mag.

sequence (ZAMS) satisfactorily lies over the observed cluster MS.

The estimation of cluster reddening values was made by taking advantage of the Magellanic Cloud extinction values based on red clump stars photometry provided by the OGLE collaboration (Udalski 2003) as described in Haschke et al. (2011). These $E(B-V)$ colour excesses are listed in Table 1. They resulted in average (0.02 ± 0.01) mag smaller than those obtained by Clementini et al. (2003). We decided not to use the Schlegel et al. (1998) full-sky maps from 100 μm dust emission, since the authors found that deviations are coherent in the sky and are especially conspicuous in regions of saturation of H I emission towards denser clouds and of formation of H_2 in molecular clouds (see also Piatti et al. 2003, 2008). We note that the small angular size of the studied clusters does not allow us to trace reddening variations in any extinction map.

For all the clusters we adopted the value of the LMC distance modulus $(m-M)_o = 18.49 \pm 0.09$ ($49.90^{-2.04}_{+2.10}$ kpc) (de Grijs et al. 2014), and an average depth for the LMC disk of (3.44 ± 1.16) kpc (Subramanian & Subramanian 2009). Bearing in mind that any cluster of the present sample could be placed in front of, or behind the LMC, we conclude that the difference in

apparent distance modulus could be as large as $\Delta(K_s - M_{K_s}) \sim 0.3$ mag, if a value of 18.49 mag is adopted for the mean LMC distance modulus. Given the fact that we estimate an uncertainty of the order of 0.3 mag when adjusting the isochrones to the cluster CMDs in magnitude, our simple assumption of adopting a unique value for the distance modulus of all the clusters should not dominate the error budget in our final results. When overplotting the ZAMS on the observed clusters' CMDs, previously shifted by the $E(B-V)$ values of Table 1 and by $(m-M)_o = 18.49$, we generally found an excellent match.

The ages and metallicities have complex and intertwined effects on the shape of the cluster's CMD. The distinction is mainly evident for the evolved RC and red giant branch (RGB) phases. The ZAMS stars are often less affected by metallicity effects and can even exhibit imperceptible variations for a specific metallicity range within the expected photometric errors. Since the LMC chemical evolution has mostly taken place within a constrained metallicity range during the last 3 Gyr, we simply used [Fe/H] values of −0.4 dex and −0.7 dex (Piatti & Geisler 2013). Further higher metallicity resolution would lead to negligible changes in the isochrones overplotted on the cluster CMDs bacause of the dispersion of the stars. We took advantage of the available theoretical isochrones computed for the VISTA photometric system to estimate cluster ages. We used recent isochrones calculated by the Padova group (Bressan et al. 2012). We then selected a set of isochrones, along with the equations $E(Y-K_s) = 0.84 \times E(B-V)$ and $K_s = M_{K_s} + (m-M)_o + 0.372 \times E(B-V)$ with $R_V = 3.1$ (Cardelli et al. 1989; Gao et al. 2013), and superimposed them on the cluster CMDs, once they were properly shifted by the corresponding $E(B-V)$ colour excesses and by the LMC apparent distance modulus. In the matching procedure, we used a subset of isochrones for each metallicity level, ranging from $\Delta(\log(t/\mathrm{yr})) = -0.3$ to +0.3 around a first rough age estimate. Finally, we adopted as the cluster age/metallicity the ones corresponding to the isochrone which best reproduced the cluster main features in the CMD. The presence of RCs and/or RGBs in some cluster CMDs made the fitting procedure easier. Table 1 lists the resulting age and metallicity values, while the bottom left panel in Fig. 3 show the corresponding isochrones superimposed to the cluster CMD (see the complete sample of clusters in Appendix A). We found that isochrones bracketing the derived mean age by $\Delta(\log(t/\mathrm{yr})) = \pm 0.1$ reasonably represent the overall age uncertainty due to the observed dispersion in the cluster CMDs, as shown in Fig. 3 (bottom left panel). Although in some cases the age dispersion is smaller than $\Delta(\log(t/\mathrm{yr})) = 0.1$, we prefer to keep the former value as an upper limit of our error budget (Piatti 2010; Piatti et al. 2011; Piatti 2014, among others). On the other hand, by assuming that both used metallicity values satisfy $\sigma([\mathrm{Fe/H}]_1 = -0.4 \text{ dex}) + \sigma([\mathrm{Fe/H}]_2 = -0.7 \text{ dex}) \geq |[\mathrm{Fe/H}]_1 - [\mathrm{Fe/H}]_2|$, and $\sigma([\mathrm{Fe/H}]_1 = \sigma([\mathrm{Fe/H}]_2$, we adopted metallicity error of $\sigma([\mathrm{Fe/H}]) = 0.15$ dex. In the case of SL 441, we found that isochrones with [Fe/H] = −0.4 dex do not satisfactorly match the cluster CMD as compared to those with solar metal content. The rather high metallicity for the LMC makes SL 441 interesting for further studies, particularly because there is no previous detailed study on this object. Nevertheless, since we are able to distinghish between isochrones with [Fe/H] = −0.3 dex and 0.0 dex, we also assume for this cluster a metallicity error of 0.15 dex.

6. Discussion

We finally estimated the ages of 65 clusters out of the 98 studied objects; 19 of them have some previous age/metallicity estimates. We have included this information in the last column of Table 1 and plotted the age differences in Fig. 5. Glatt et al. (2010) used data from the Magellanic Cloud Photometric Surveys (Zaritsky et al. 2002) to build cluster CMDs and to derive their ages from theoretical isochrone fits. Although they mention that field contamination is a severe effect in the extracted cluster CMDs and therefore influences the age estimates, no decontamination from field CMDs were carried out. Consequently, their large age errors could reflect the composite LMC stellar populations. Thus, as an example, they estimated for HS 232 an age of $\log(t/\mathrm{yr}) = 9.2 \pm 0.1$, whereas from our analysis we could not confirm the object to be a possible star cluster. Likewise, from a total of 14 clusters in common, we found a difference of $|\log(t/\mathrm{yr})_{\mathrm{glatt}} - \log(t/\mathrm{yr})_{\mathrm{our}}| = 0.3 \pm 0.4$ (absolute values). For the remaining five clusters with previous age estimates, we found an excellent agreement (see Table 1).

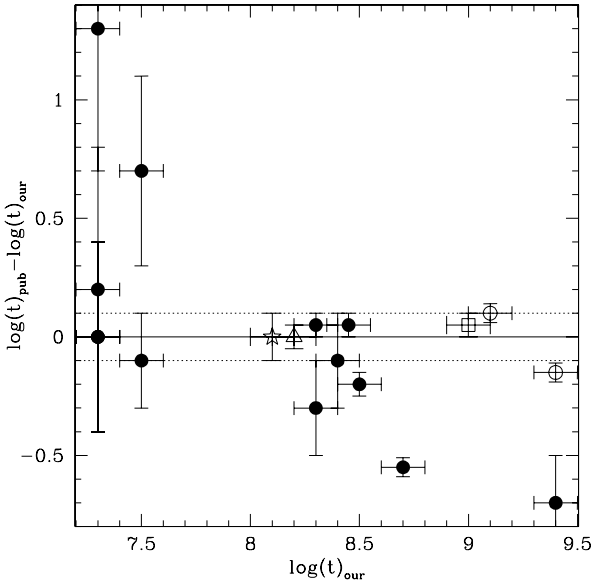

Fig. 5. Age difference between present age estimates and those published by Glatt et al. (2010, filled circle), Piatti (2011, open circle), Milone et al. (2009, open box), Gouliermis et al. (2010, open triangle), and Piatti (2012, open star). The vertical errorbars represent the age uncertanties from the published values.

For the metallicity estimates, Glatt et al. (2010) adopted a value of [Fe/H] = −0.4 dex for the 14 clusters in common, which is in excellent agreement with our values except for SL 435, for which we used a more metal-poor isochrone ([Fe/H] = −0.7 dex). We think that the difference in metallicty for SL 435 could be due to field contamination effects as mentioned above, since the cluster age also differs significantly. Three other clusters with metallicity values published in the literature are NGC 1987, NGC 2010, and SL 510. Milone et al. (2009) obtained the best isochrone fit to the NGC 1987 CMD using $Z = 0.010$ ([Fe/H] = −0.3 dex), while Gouliermis et al. (2010) and Piatti (2012) assumed a metallicity of [Fe/H] = −0.4 dex for NGC 2010 and SL 510. As can be seen, our present values are in excellent agreement with those previously published. On the other hand, the percentage of clusters with [Fe/H] = −0.7 dex resulted in nearly the same value for both tiles (≈20%), as well as the mean cluster metallicities ([Fe/H] = −0.45 ± 0.15 dex); the number of more metal-rich clusters is higher in tile LMC 5_5 than in tile LMC 8_8.

The catalogued objects SL 528 and OGLE 545 are two objects located very close to each other in the sky (angular separation ≈0.55′) whose decontaminated CMDs look very similar.

They do not show the cluster MSs, but exhibit visible RCs. We interpret this effect either as coming from our not-deep-enough photometry of intermediate-age clusters ($\log(t/\mathrm{yr}) > 9$) or as dealing with cluster-like asterisms, i.e, as a statistical fluctuation of the field or a low-absorption window (Bica & Bonatto 2011). The catalogued cluster candidate BSDL 1182 also has a decontaminated CMD similar to those of SL 528 and OGLE 545. However, in this case we think that we are dealing with a group of RC stars or with an unresolved star cluster. We note that in order to asses the objects' reality we used the information coming from the CMDs and from the spatial distributions.

As far as we are aware, the most recent catalogue of LMC star clusters which puts all the previous ones together is that of B08. Although it is expected that most of the catalogued objects are indeed genuine physical systems, it was beyond the scope of B08 to verify the physical nature of such faint objects. The task of cleaning cluster catalogues from non-physical systems or asterisms is far from being an exciting job. For this reason studies concluding about the asterism or overdensity nature of faint objects in the Clouds are rare or absent (Piatti & Bica 2012). However, this analysis is very important and would be required for any statistical analysis of the cluster formation and disruption rates, the cluster spatial, age, and metallicity distributions, etc., is attempted. Since the B08 catalogue was compiled from previously existing catalogues built on the basis of star counts, either by visually inspecting photographic plates (Bruck 1975; Hodge 1986; Bica & Schmitt 1995, for example) or by automatic algorithmic searches (Pietrzynski et al. 1999, for example), we should not rule out the possible occurrence of such asterisms.

Indeed, we classified 19 of the studied objects as possible non-clusters. For them, although apparent concentrations of stars in a typically 1′ wide angular region can be observed in the K_s images, a careful inspection of the resulting spatial distributions and the decontaminated CMDs for stars with $P(\%) > 75$ did not allow us to firmly conclude that they are genuine physical systems. However, the present analytical tools applied to faint poorly populated clusters or candidates in the LMC point to the need of higher spatial resolution and deeper observations with e.g. the 8 m class telescopes. For eight objects, we could not find a clear star concentration in the K_s images either, so that we quoted them as cluster-like asterisms in Table 1. Finally, we found two previously catalogued single star clusters to be unresolved background galaxies on the basis of isophote analyses and the comparison of radial profiles of a sample of objects in the images (KMHK 747, OGLE 366) and a triple cluster system (BSDL 2144: (RA, Dec) ≈ (05:31:10.0, −71:08:00.0), (05:31:08.0, −71:07:50.0), and (05:31:05.0, −71:07:55.0)). Nevertheless, better spatially resolved images are needed in order to give more conclusive results. Instead of building their schematic charts and CMDs, we provide the respective K_s images (see Fig. 6). We have superimposed isophotes curves which highlight the unresolved nature of these objects. For comparison purposes we include an enlargment of the K_s image centred on the cluster SL 435 in the bottom right panel of Fig. 6 (see also Fig. 3).

Piatti (2014) showed that there are some variations in the LMC star cluster frequency (CF) in terms of cluster spatial distribution. Particularly he found that 30 Doradus turns out to be the region with the highest relative frequency of the youngest clusters, while the $\log(t/\mathrm{yr}) = 9{-}9.5$ (1−3 Gyr) age range is characterised by cluster formation at a higher rate in the inner regions than in the outer ones. In Fig. 7 we compare the CF we obtained for the tile LMC 5_5 to those obtained by Piatti (2014) for the Bar and the outer Bar, since this tile covers regions of both structures (Harris & Zaritsky 2009; Moretti et al. 2014). When building the CF we took into account the same precepts outlined in Piatti (2014), i.e. the influence of adopting arbitrary age bins, as well as the fact that each age value is associated to an uncertainty which allows the age value to fall centred on an age bin or outside it. In practice, we varied the bin size based on the average error of the age of the clusters that fall in each bin, thus tracing the variation of the age uncertainties along the whole age range. In addition, even though the age bins are set to match the age errors, any individual point in the CF may fall into the respective age bin or either of the two adjacent bins. This happens when an age point does not fall in the bin centre and, owing to its errors, has the chance of falling outside it. For this reason, we weighed the contribution of each age value – a segment with size 2σ(age) – to each one of the age bins occupied by it, so that the sum of all the weights equals unity. We performed thus a robust procedure which takes into account both effects, the age bin size and the age errors. Since the total number of clusters in the tile and in the sample used by Piatti (2014) is different, we normalised the CF to the total number of clusters employed, for comparison purposes. We note that we are interested in comparing the slope or changes in the CF rather than the total number of clusters formed per age interval. Although tile LMC 5_5 encompasses a small portion of the LMC outer Bar/Bar (see Fig. 1), we found that its CF is comparable to those of the outer Bar and the Bar. These results might reflect that the different parts of the LMC outer Bar/Bar have behaved in a similar way forming star clusters during the last 1−2 Gyr. We did not, however, measure ages of clusters older than ∼log(t/yr) = 9.6 (4 Gyr) which, in turn, might suggest that old clusters are not as homogeneously distributed as those younger ones in terms of CF in the inner LMC regions.

7. Conclusions

In this work we analyse CMDs of catalogued star clusters located in the LMC from a YJK_s photometric dataset obtained by the VISTA VMC collaboration. We focused on tiles LMC 5_5 and 8_8 because they are among the first completed by the VMC survey for which we obtained PSF photometry. Since they are, respectively, located towards a LMC outer Bar/Bar and SEP regions, we could assess the performance of estimating ages for the oldest clusters observed (i.e. limiting magnitude reached) in relatively crowded and uncrowded fields. We analysed a total of 98 catalogued clusters of small angular size, typically ∼11.6 pc in diameter.

We applied a subtraction procedure developed by Piatti & Bica (2012) to statistically clean the cluster CMDs from field star contamination in order to disentangle cluster features from those belonging to their surrounding fields. The employed technique makes use of variable cells in order to reproduce the field CMD as closely as possible.

From matching theoretical isochrones computed for the VISTA system to the cleaned cluster CMDs we estimated ages and metallicities. When adjusting a subset of isochrones we took into account the LMC distance modulus and the individual star cluster colour excesses. We finally estimated the ages of 65 clusters out of the 98 studied objects, which are in the age range $7.3 < \log(t/\mathrm{yr}) < 9.55$. This cluster sample will be part of the cluster data base that the VMC survey will produce in order to homogeneously study the overall cluster formation history throughout the Magellanic system.

We also classified 19 of the studied objects as possible non-clusters (e.g. chance grouping of stars) since a careful

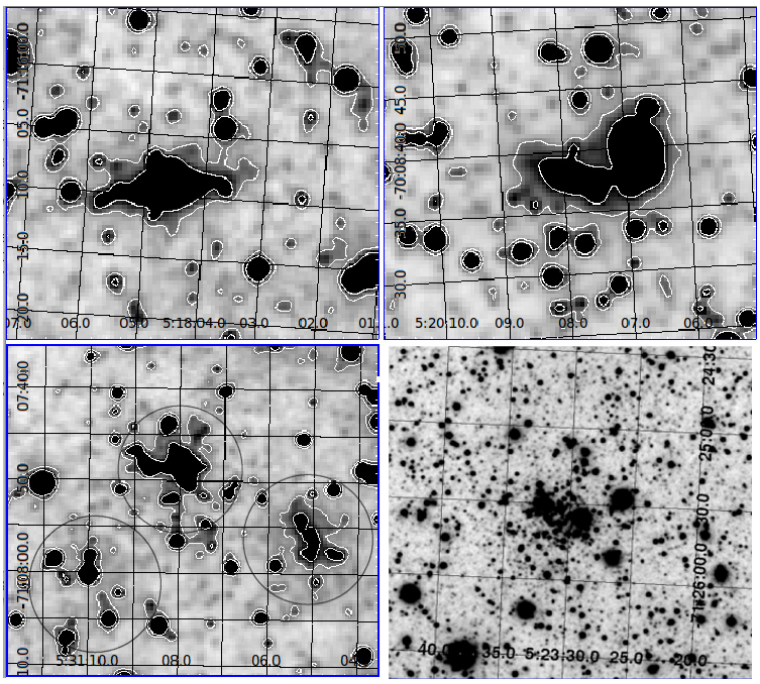

Fig. 6. Enlargement of K_s images of tile LMC 5_5 centred on KMHK 747 (*top left*, possible galaxy), OGLE 366 (*top right*, possible galaxy), BSDL 2144 (*bottom left*, possible triple system), and SL 435 (*bottom right*). Isophote curves have been superimposed.

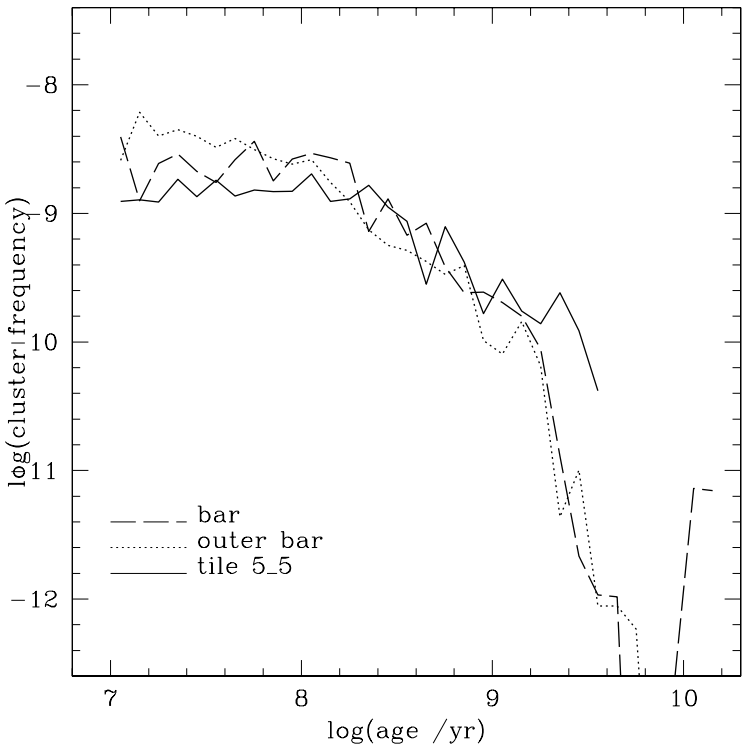

Fig. 7. Cluster frequencies for the LMC outer Bar, Bar, and tile LMC 5_5 (see text for details).

inspection of the resulting spatial distributions and the decontaminated CMDs for stars with probabilities of being a fiducial cluster feature higher than 75% did not allow us to firmly conclude that they are genuine physical systems. Two other objects were classified as possible cluster-like asterisms and another one as an unresolved cluster. For another eight objects, we could not find a clear star concentration in the K_s images, so we listed them as cluster-like asterisms. Finally, we found two previously catalogued single star clusters to be unresolved background galaxies (KMHK 747, OGLE 366) and a triple cluster system (BSDL 2144).

Acknowledgements. We thank the Cambridge Astronomy Survey Unit (CASU) and the Wide-Field Astronomy Unit (WFAU) in Edinburgh for providing calibrated data products under the support of the Science and Technology Facility Council (STFC) in the UK. This research has made use of the SIMBAD database, operated at CDS, Strasbourg, France. This work was partially supported by the Argentinian institutions CONICET and Agencia Nacional de Promoción Científica y Tecnológica (ANPCyT). R.G. is a Postdoctoral Fellow – Pegasus of the Fonds Wetenschappelijk Onderzoek (FWO) – Flanders. R.d.G. acknowledges research support from the National Natural Science Foundation of China (NSFC) through grant 11373010. G.C. acknowledges research support from PRIN-INAF 2010 (P. I. G. Clementini). B.-Q. F. is the recipient of a John Stocker Postdoctoral Fellowship from the Science and Industry Endowment Fund. We thank the anonymous referee whose comments and suggestions allowed us to improve the manuscript.

Appendix A: Complete sample of clusters

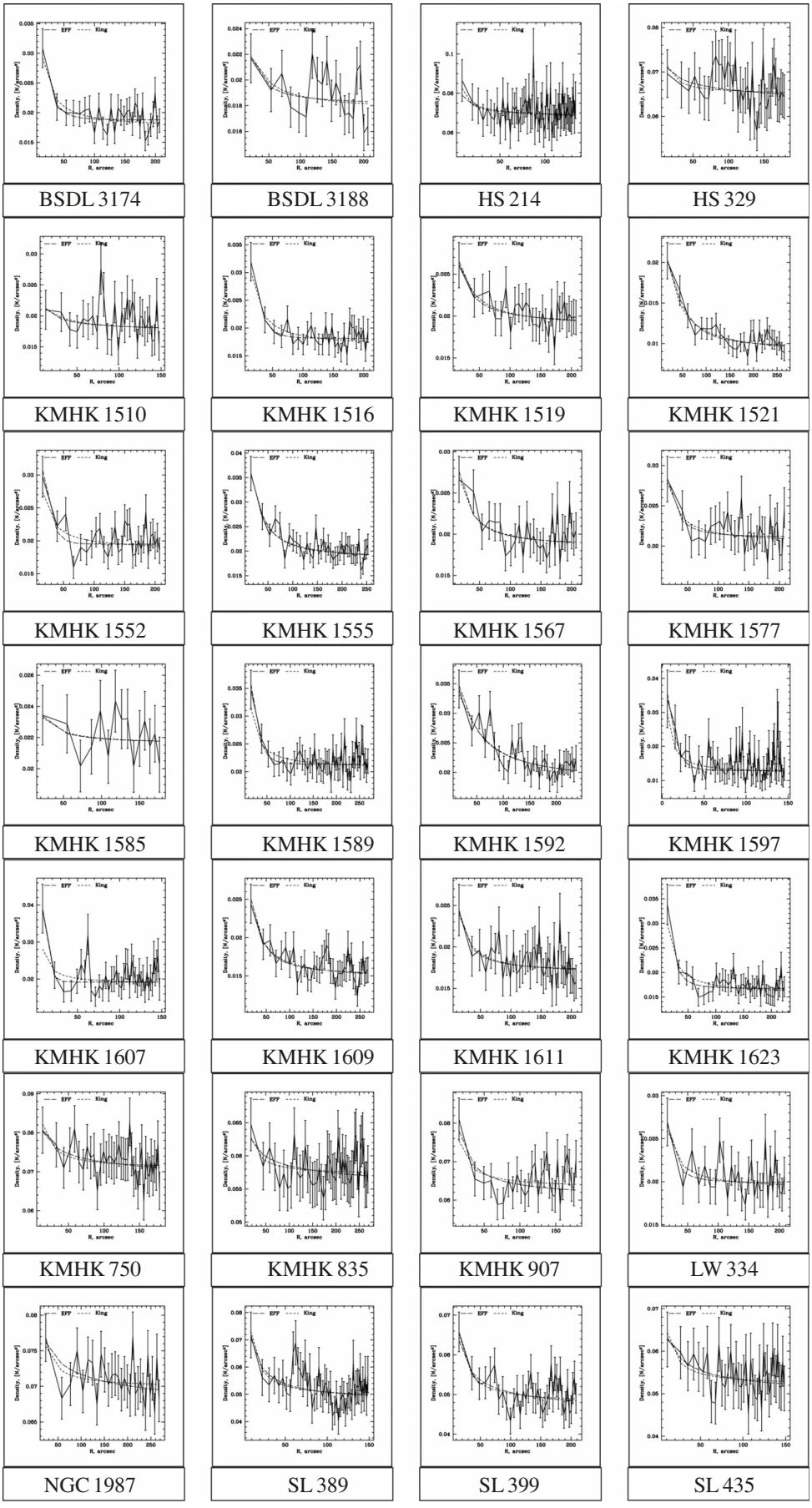

Fig. A.1. Radial profiles of the clusters (see details in Sect. 4.1).

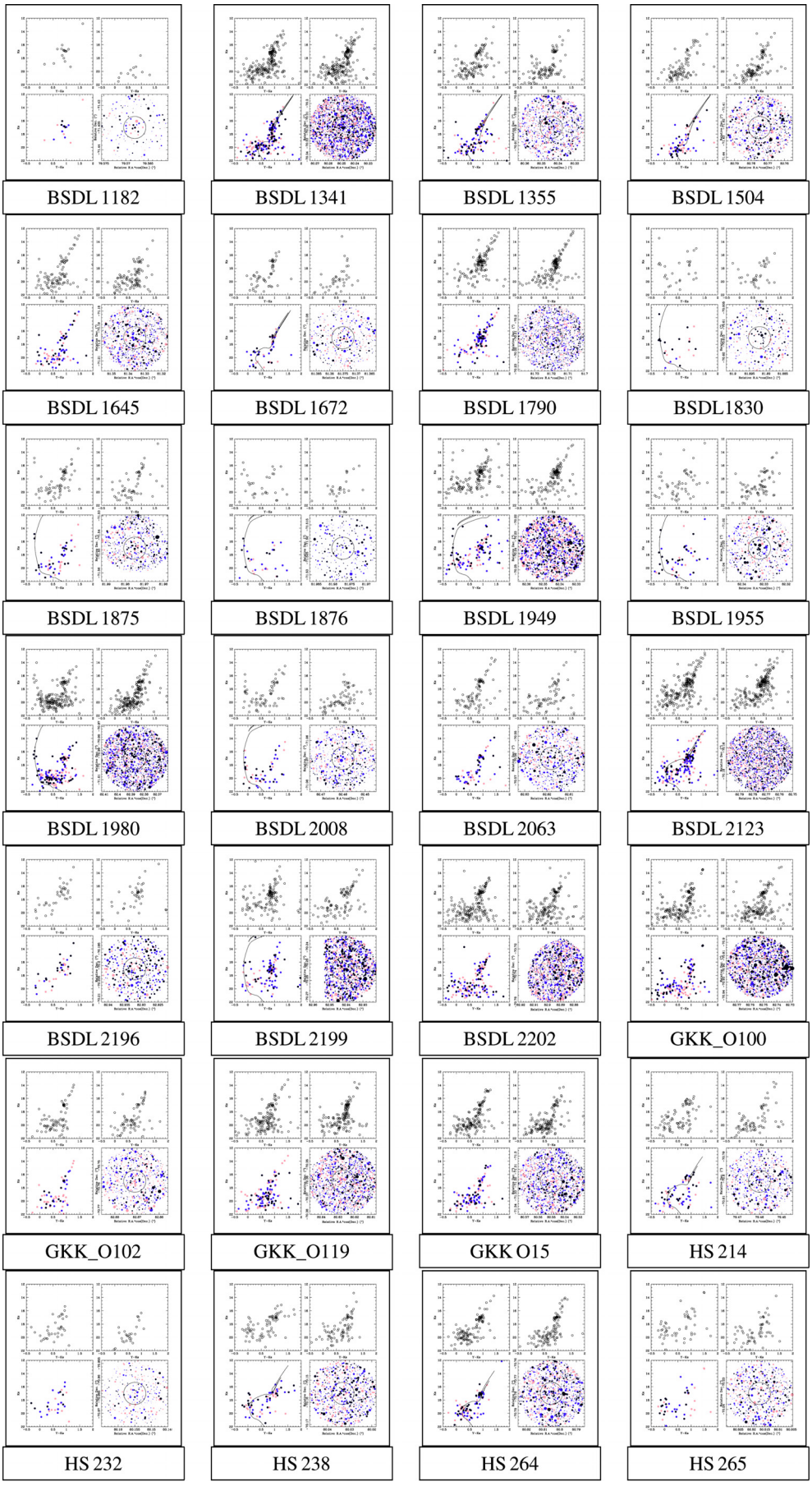

Fig. A.2. CMDs of the cluster sample (see details in Sect. 5).

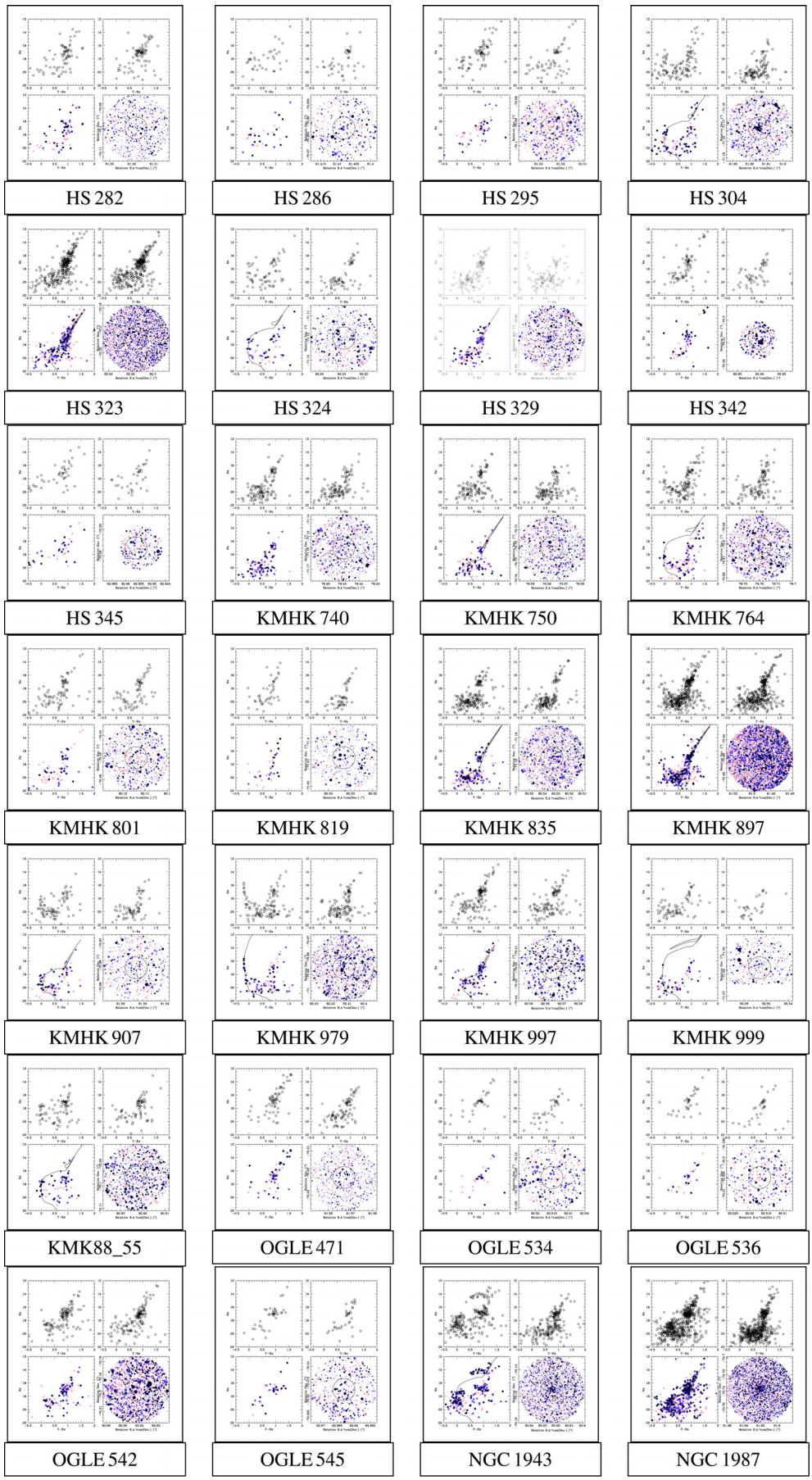

Fig. A.3. CMDs of the cluster sample (see details in Sect. 5).

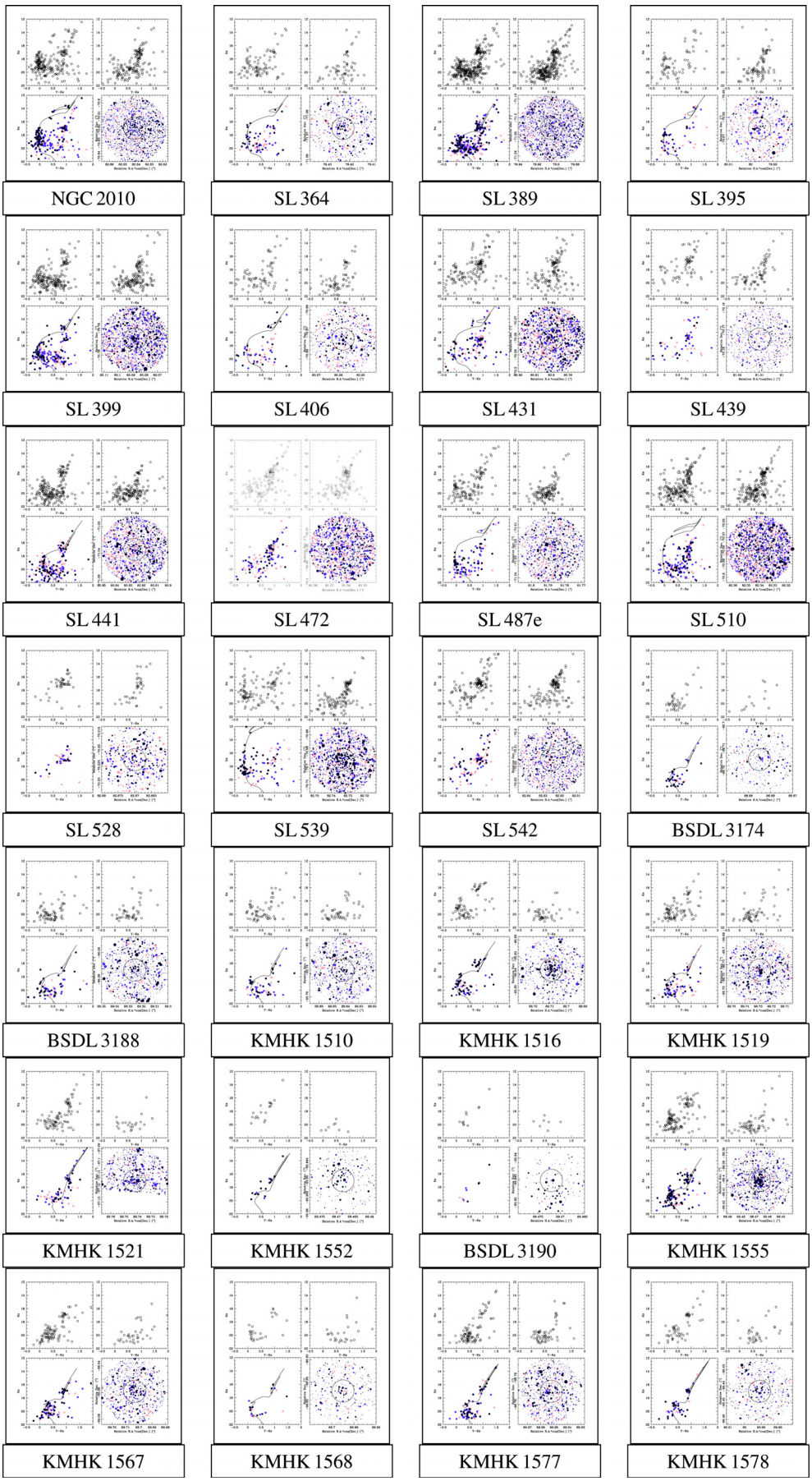

Fig. A.4. CMDs of the cluster sample (see details in Sect. 5).

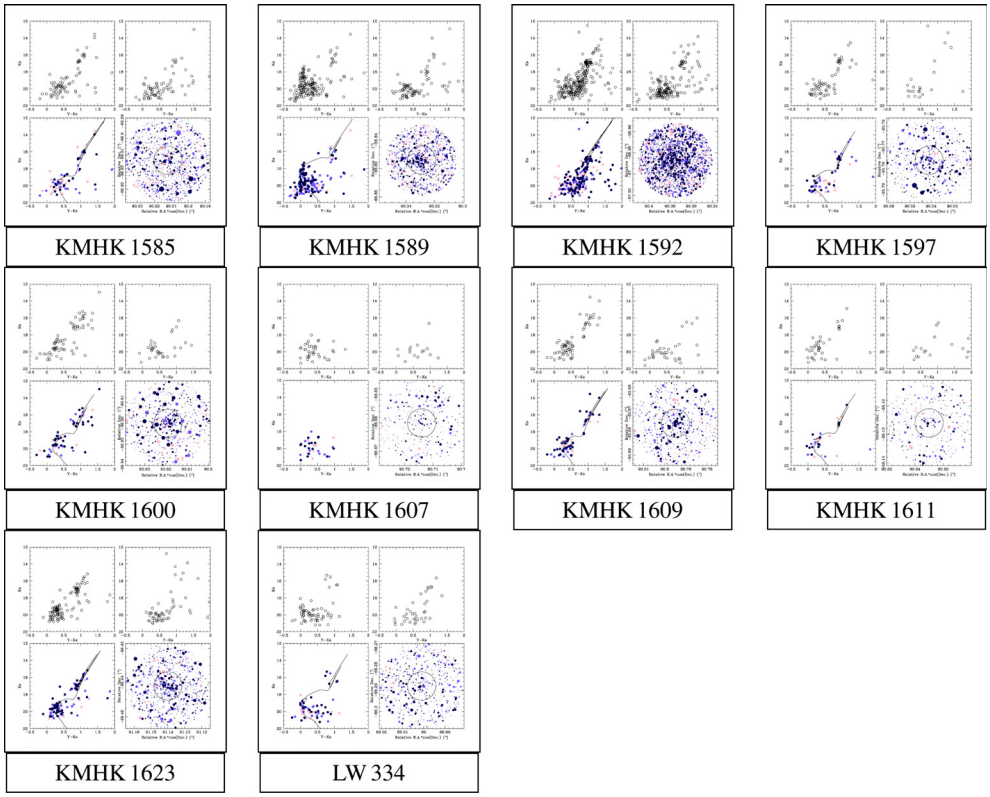

Fig. A.5. CMDs of the cluster sample (see details in Sect. 5).

References

Baumgardt, H., Parmentier, G., Anders, P., & Grebel, E. K. 2013, MNRAS, 430, 676
Bica, E., & Bonatto, C. 2011, A&A, 530, 32
Bica, E., & Schmitt, H. R. 1995, ApJS, 101, 41
Bica, E., Bonatto, C., Dutra, C. M., & Santos Jr., J. F. C. 2008, MNRAS, 389, 678
Bressan, A., Marigo, P., Girardi, L., et al. 2012, MNRAS, 427, 127
Bressan, A., Marigo, P., Girardi, L., Nanni, A., & Rubele, S. 2013, EPJ Web Conf., 43, 03001
Bruck, M. T. 1975, MNRAS, 173, 327
Cardelli, J. A., Clayton, G. C., & Mathis, J. S. 1989, ApJ, 345, 245
Clementini, G., Gratton, R., Bragaglia, A., et al. 2003, AJ, 125, 1309
Cioni, M. R., Clementini, G., Girardi, L., et al. 2011, A&A, 527, A116
Cross, N. J. G., Collins, R. S., Mann, R. G., et al. 2012, A&A, 548, A119
Da Rio, N., Gouliermis, D. A., & Henning, Th. 2009, ApJ, 696, 528
de Grijs, R., & Anders, P. 2006, MNRAS, 366, 295
de Grijs, R., & Goodwin, S. P. 2008, MNRAS, 383, 1000
de Grijs, R., Goodwin, S. P., & Anders, P. 2013, MNRAS, 436, 136
de Grijs, R., Wicker, J. E., & Bono, G. 2014, AJ, 147, 122
Dieball, A., Müller, H., & Grebel, E. K. 2002, A&A, 391, 547
Elson, R. A. W., Fall, S. M., & Freeman, K. C. 1987, ApJ, 323, 54
Gao, J., Jiang, B. W., Li, A., & Xue, M. Y. 2013, ApJ, ApJ, 776, 7
Glatt, K., Gallagher, J. S. III, Grebel, E. K., et al. 2008, AJ, 135, 1106
Glatt, K., Grebel, E. K., & Koch, A. 2010, A&A 517, 50
Gouliermis, D. A., Mackey, D., Xin, Y., & Rochau, B. 2010, ApJ, 709, 263
Haschke, R., Grebel, E., & Duffau S. 2011, AJ, 141, 158
Harris, J., & Zaritsky, D. 2009, AJ, 138, 1243
Hill, A., & Zaritsky, D. 2011, AJ, 131, 414
Hodge, P. W. 1986, PASP, 98, 1113
Indu, G., & Subramaniam, A. 2011, A&A, 535, A115
Irwin, M. J., Lewis, J., Hodgkin, S., et al. 2004, in SPIE Conf. Ser. 5493, eds. P. J. Quinn, & A. Bridger, 411
King, I. 1962, AJ, 67, 471
Kontizas, M., Morgan, D. H., Hatzidimitriou, D., & Kontizas, E. 1990, A&AS, 84, 527
Lewis, J. R., Irwin, M., & Bunclark P. 2010, in Astronomical Data Analysis Software and Systems XIX, eds. Y. Mizumoto, K.-I. Morita, M. Ohishi (San Francisco: ASP), ASP Conf. Ser., 434, 91
Marigo, P., Girardi, L., Bressan, A., et al. 2008, A&A, 482, 883
Milone, A. P., Bedin, L. R., Piotto, G., & Anderson, J. 2009, A&A, 497, 755
Moretti, M. I., Clementini, G., Muraveva, T., et al. 2014, MNRAS, 437, 2702
Nikolaev, S., & Weinberg, M. D., ApJ, 542, 804
Piatti, A. E. 2010, A&A, 513, L13
Piatti, A. E. 2011, MNRAS, 418, L40
Piatti, A. E. 2012, A&A, 540, A58
Piatti, A. E. 2014, MNRAS, 437, 1646
Piatti, A. E., & Bica, E. 2012, MNRAS, 425, 3085
Piatti, A. E., & Geisler, D. 2013, AJ, 147, 17
Piatti, A. E., Sarajedini, A., Geisler, D., Bica, E., & Clariá, J. J. 2002, MNRAS, 329, 556
Piatti, A. E., Clariá, J. J., & Ahumada, A. V. 2003, MNRAS, 340, 1249
Piatti, A. E., Geisler, D., Sarajedini, A., Gallart, C., & Wischnjewsky, M. 2008, MNRAS, 389, 429
Piatti, A. E., Clariá, J. J., Bica, E., et al. 2011, MNRAS, 417, 1559
Pietrzyński, G., Udalski, A., Kubiat, M., et al. 1999, Acta Astron., 49, 521
Pietrzyński, G., Graczyk, D., Gieren, W., et al. 2013, Nature, 495, 76
Popescu, B., & Hanson, M. M., 2009, AJ, 138, 1724
Rubele, S., Kerber, L., Girardi, L., et al. 2012, A&A, 537, A106
Schlegel, D. J., Finkbeiner, D. P., & Davis, M. 1998, ApJ, 500, 525
Stetson, P. B. 1987, PASP, 99, 191
Subramanian, S., & Subramanian, A. 2009, A&A, 496, 399
Tatton, B., van Loon, J. Th., Cioni, M. R., et al. 2013, A&A, 554, A33
Udalski, A. 2003, Acta Astron., 53, 291
van der Marel, R. 2001, AJ, 122, 1827
Werchan, F., & Zaritsky, D. 2011, AJ, 142, 48
Zaritsky, D., Harris, J., Thompson, I. B., Grebel, E. K., & Massey, P. 2002, AJ, 123, 855
Zaritsky, D., Harris, J., & Thompson, I. B., et al. 2004, AJ, 128, 1606